Research Square

Preprints are preliminary reports that have not undergone peer review.
They should not be considered conclusive, used to inform clinical practice,
or referenced by the media as validated information.

Tying Molecular 85 and 51 Knots via Aza-Indolyl Motif

Guo-Xin Jin

gxjin@fudan.edu.cn

Fudan University https://orcid.org/0000-0002-7149-5413

Yan Zou

Fudan University

Haitong Tang

Fudan University

Article

Keywords:

Posted Date: April 29th, 2026

DOI: https://doi.org/10.21203/rs.3.rs-9478474/v1

License: This work is licensed under a Creative Commons Attribution 4.0 International License.
Read Full License

Additional Declarations: There is **NO** Competing Interest.

Tying Molecular 8_5 and 5_1 Knots via Aza-Indolyl Motif

Yan Zou[a,+], Haitong Tang[a,+], and Guo-Xin Jin[a,b,*]

[a]Shanghai Key Laboratory of Molecular Catalysis and Innovative Materials, State Key Laboratory of Molecular Engineering of Polymers, Department of Chemistry, Fudan University, Shanghai 200433, P. R. China
[+]These authors contributed equally to this work
*E-mail: gxjin@fudan.edu.cn.

[b]State Key Laboratory of Coordination Chemistry, School of Chemistry and Chemical Engineering, Nanjing University, Nanjing, 210093, P. R. China
*E-mail: gxjin@fudan.edu.cn.

Abstract: The synthesis of molecular topology beyond conventional symmetric knots remains a formidable challenge. Here, we report the first synthesis of the molecular 8_5 knot—a low-symmetry, representative pretzel knot with eight crossing points—via coordination-driven self-assembly. This knot was assembled from eight 4-azaindolyl ligand strands (**L**) and eight binuclear metal blocks (**E1-Rh)**. These components intertwine in three-dimensional space in an alternating up-and-down fashion, forming a closed loop featuring eight crossings. Successful construction of this elusive 8_5 knot relies on our newly developed 4-azaindolyl ligand strand, whose unique electronic and steric properties enable tunable topological organisation. Exploiting this ligand design, we further systematically synthesized two 5_1 torus knots in high yields by tuning the size of the binuclear metal motifs, thereby validating the platform's broad applicability. This study fills a key gap concerning low-symmetry eight-crossing molecular knots and establishes a versatile route to accessing diverse molecular topologies.

Main

Molecular knots[1-3], a class of topologically non-trivial supramolecular architectures characterized by entangled closed-loop molecular backbones with well-defined crossing points, have emerged as a vibrant frontier in modern supramolecular chemistry, owing to their unique topological aesthetics and promising applications in information storage,[4,5] molecular recognition,[6,7] and catalysis.[8,9] The first synthesis of a molecular knot (trefoil knot, 3_1 in Alexander–Briggs notation[10]) was realized by Sauvage and co-workers in 1989.[11] Since then, progressive refinements to targeted synthetic methodologies[12-14] have driven major advances in the field, yielding a growing library of non-trivial knots ranging from simple trefoil knot (3_1)[15,16] and figure-eight knot (4_1)[17,18] to more complex 5_1 knot,[19] 7_1 knot,[20] and beyond[14].

Eight-crossing prime knots represent a rare and underexplored class of architectures, as their synthesis requires precise control over ligand-folding conformations, coordination-site matching, and strand entanglement, with only a handful reported to date. In 2017, Leigh et al. synthesized the first eight-crossing 8_{19} molecular knot with topological chirality, using a triple-helix braiding strategy based on dynamic terpyridine–iron(II) coordination (Fig. 1a).[21] Our group constructed a well-defined 8_{18} metalla-knot in 2021 via conventional pyridyl ligand-based self-assembly[22], establishing the efficiency and high-yield nature of this approach for accessing higher-order topologies (Fig. 1b). Although the family of eight-crossing prime knots comprises 21 distinct topological isomers, only the above two symmetric topologies have been successfully synthesized with small molecules to date; all other low-symmetry architectures remain elusive. Among these, the 8_5 knot—an alternating prime knot classified as the pretzel knot *P* (3,3,2) in knot theory[23]—is of unique structural and topological interest. Topologically, the 8_5 knot has a minimal crossing number of eight, with three twisted bands containing three, three, and two positive half-twists, respectively. Furthermore, it has three mutually perpendicular C_2 rotation axes and exhibits chirality, slice-knot characteristics, and well-defined polynomial invariants, making it an ideal model to probe topology–function relationships at the molecular level.

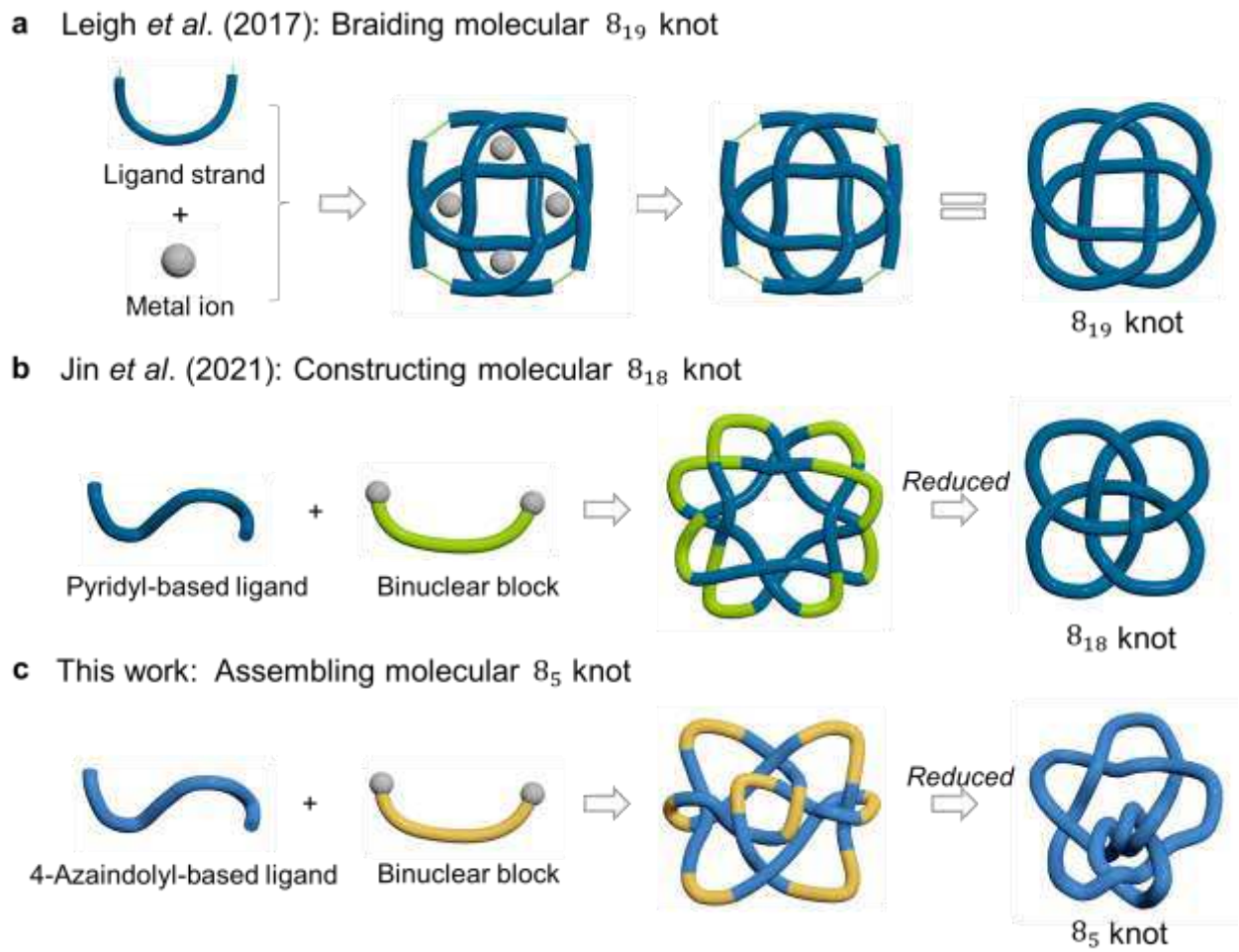


Fig. 1 | Synthetic schematic of molecular knots with an eight-crossing point. a, Leigh's group assembles an 8_{19} knot from a metal template strategy. **b**, Jin's group synthesizes an 8_{18} knot through a coordination-driven self-assembly method based on a pyridyl ligand. **c**, A novel 8_5 knot was synthesized by a 4-azaindolyl-based ligand strand.

Coordination-driven self-assembly represents a powerful tool for constructing complex topological architectures, capitalizing on the dynamic and reversible nature of metal–ligand bonds.[24-26] Our group has long specialized in employing pyridyl-based ligand strands to assemble diverse complex topologies via coordination-driven self-assembly[27,28]; however, the fixed coordination modes and spatial-directing effects of traditional pyridyl ligands often restrict access to a limited set of symmetric topologies. Consequently, there is a pressing need for new ligand platforms with tailored coordination motifs that enable the rational assembly of complex, low-symmetry topological species.

Herein, we present a systematic study centred on an innovative coordination motif to achieve the synthesis of different prime knots (Fig. 2a). We designed novel 4-azaindolyl-based bidentate

ligands possessing significantly different electron properties, coordination angles, and steric profiles compared to pyridyl-based ligands.[29-31] This pivotal alteration successfully directed the selective synthesis of an eight-crossing 8_5 molecular knot in high yield (Figs. 1c and 2b). Single-crystal X-ray diffraction (SCXRD) analysis unambiguously confirmed its precise topology, which is an isocrossing knot of the reported 8_{19} and 8_{18} knots, but undergoes a completely different self-assembly pathway and entanglement mode. Crucially, this 4-azaindolyl-based ligand system exhibits remarkable versatility. Using the same ligand strand, we further successfully synthesized two five-crossing 5_1 torus knots via size-directed approaches (Fig. 2b). This work not only realizes the first chemical synthesis of the 8_5 knot but also, more fundamentally, pioneers and verifies a powerful coordination motif, thereby overcoming the limitations of traditional paradigms and enabling the directed synthesis of other higher-order molecular architectures.

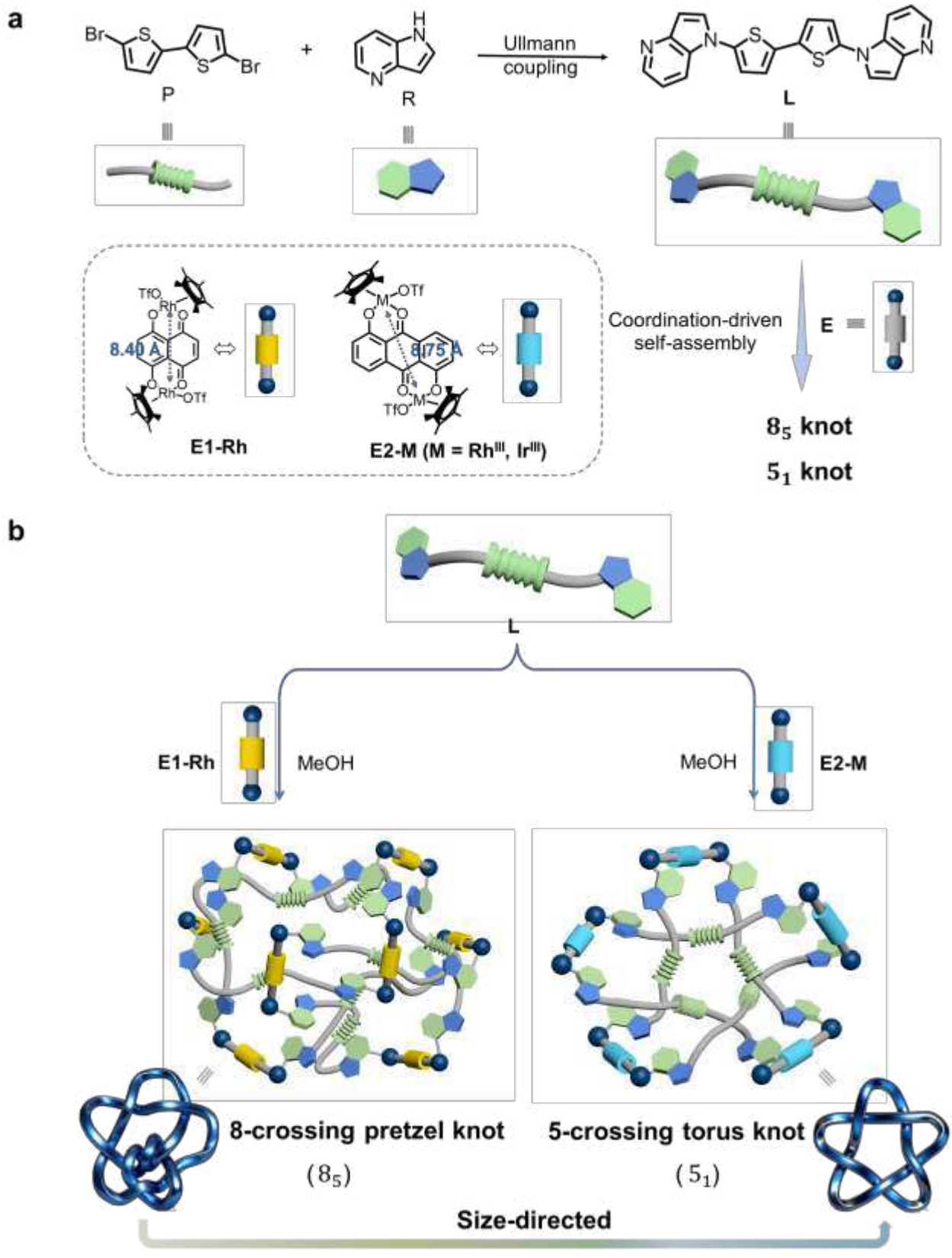


Fig. 2 | Synthetic the molecular 8_5 knot, and 5_1 knot. a, Strategies for designing molecular knots. **b**, A summary diagram of molecular 8_5 knot and 5_1 knot was synthesized based on the 4-azaindolyl-based ligand strands.

Results and Discussion

A new 4-azaindolyl motif for the synthesis of 8_5 knot 1

Ligand **L** was synthesized via copper-catalyzed Ullmann coupling between 4-azaindole and 5,5'-dibromo-2,2'-bithiophene at 160°C in *N,N*-dimethylformamide (DMF) for 72h (Supplementary Figs. 1 and 4–7). Subsequent treatment with an equimolar amount of the Cp*Rh-containing binuclear block **E1-Rh** (Rh···Rh separation 8.40 Å) in methanol yielded a clear green solution, and precipitation with diethyl ether afforded the target product as a green crystalline solid in a 70% yield (Fig. 3a). Electrospray ionization time-of-flight mass spectrometry (ESI-TOF/MS) confirmed the formation of hexadecanuclear complex **1**, with the characteristic peaks detected at *m/z* 2028.4919 and 2572.8611, assigned to the species $[(\mathbf{E1\text{-}Rh})_8(\mathbf{L})_8](OTf^-)_n$ (n = 11, 12) (Figs. 3c, 3d, and Supplementary Figs. 12–14). The ^{1}H NMR spectrum of **1** in methanol-d_4 at 298.15K reveals it to have a low-symmetry topology, in which the eight ligand strands occupy four different chemical environments in a 2:2:2:1 integral ratio (Supplementary Figs. 8, 9, and 11), and diffusion-ordered spectroscopy (DOSY) further verified the formation of a single species with a self-diffusion constant of $D = 1.94 \times 10^{-10}$ m^2 s^{-1} (Fig. 3e and Supplementary Fig. 10).

To unambiguously establish its topological architecture and entanglement mode, single crystals suitable for X-ray diffraction were grown via solvent diffusion of diethyl ether into a concentrated methanolic solution of **1**, affording green block-shaped crystals over several days. The X-ray diffraction data confirm that the compound adopts an unprecedented low-symmetry 8_5 molecular knot topology, with a closed metal–organic strand crossing eight times (Fig. 3b). The 8_5 knot, the fifth prime knot in the Rolfsen table of eight-crossing knots, is a paradigmatic topological structure holding profound significance in both knot theory and supramolecular chemistry. As an alternating 3-braid prime knot, it admits two canonical tangle-based constructions: it can be realized as the numerator closure of the sum of rational tangles 30 + 30 + 20, and is equivalently classified as the *P*(3,3,2) pretzel knot, formed by performing the "multiplication by 0" operation on three sub-tangles with 3, 3, and 2 twists, respectively, followed by horizontal addition and closure[23]. Furthermore, the dimensions of the solid-state structure of **1** were measured (height × diameter, 34.84 Å × 33.75 Å), agreeing with the hydrodynamic size calculated from the diffusion constant ($D = 1.94 \times 10^{-10}$ m^2 s^{-1}) in the ^{1}H DOSY NMR spectrum via the modified Stokes–Einstein equation based on the cylinder model (Fig. 3f and Supplementary Fig. 46). This intricate architecture is

formed by eight ligand strands (**L**) interweaving in three-dimensional space, which are subsequently linked and capped by binuclear blocks (**E1-Rh**) via coordination bonds, resulting in an internally entwined framework incorporating eight crossings (Figs. 4a–c). The ligand strand **L** incorporates a central bithiophene motif, a unit intrinsically capable of adopting both *s-cis* and *s-trans* conformations with different Rh···Rh separations ranging from 18.11 Å to 19.46 Å (Fig. 4e and Supplementary Figs. 33, 34).

In the free ligand and conventional supramolecular assemblies, the *s-trans* conformation is energetically preferred, driven by minimizing the steric repulsion between the lone pairs of the sulfur atoms.[32] Strikingly, single-crystal structural analysis of the 8_5 knot reveals a selective, orientation-dependent conformational differentiation among its eight ligand strands: those aligned along the longitudinal axis of the architecture partially adopt the *s-cis* conformation, stabilized by the rigid coordination environment, whereas all the strands aligned along the transverse axis retain the thermodynamically favourable *s-trans* conformation (Figs. 4d and 4f). The corresponding S–C–C–S torsion angles of the bithiophene core range from 21.46° to 26.70° for the *s-cis* conformation, and from 152.45° to 179.77° for the *s-trans* conformation. This highly selective conformational distribution within the complex topological framework is not preorganized. Instead, it arises from an adaptive conformational selection during the coordination-driven self-assembly process, wherein the ligand strands dynamically adjust their geometries to satisfy the strict spatial constraints required for the ordered topological entanglement.

The solution stability of **1** was systematically evaluated using variable-concentration ^{1}H NMR experiments (Supplementary Fig. 30). In methanol-d_4, as the solution was gradually diluted from 2.50 mM to 0.01 mM, the chemical shifts (δ) of all characteristic proton signals remained constant, with no detectable variations in peak splitting patterns or relative integral ratios. This remarkable spectral consistency across a 250-fold concentration range indicates that the molecular topology of **1** remains intact in solution, precluding any detectable dissociation or rearrangement occurring.

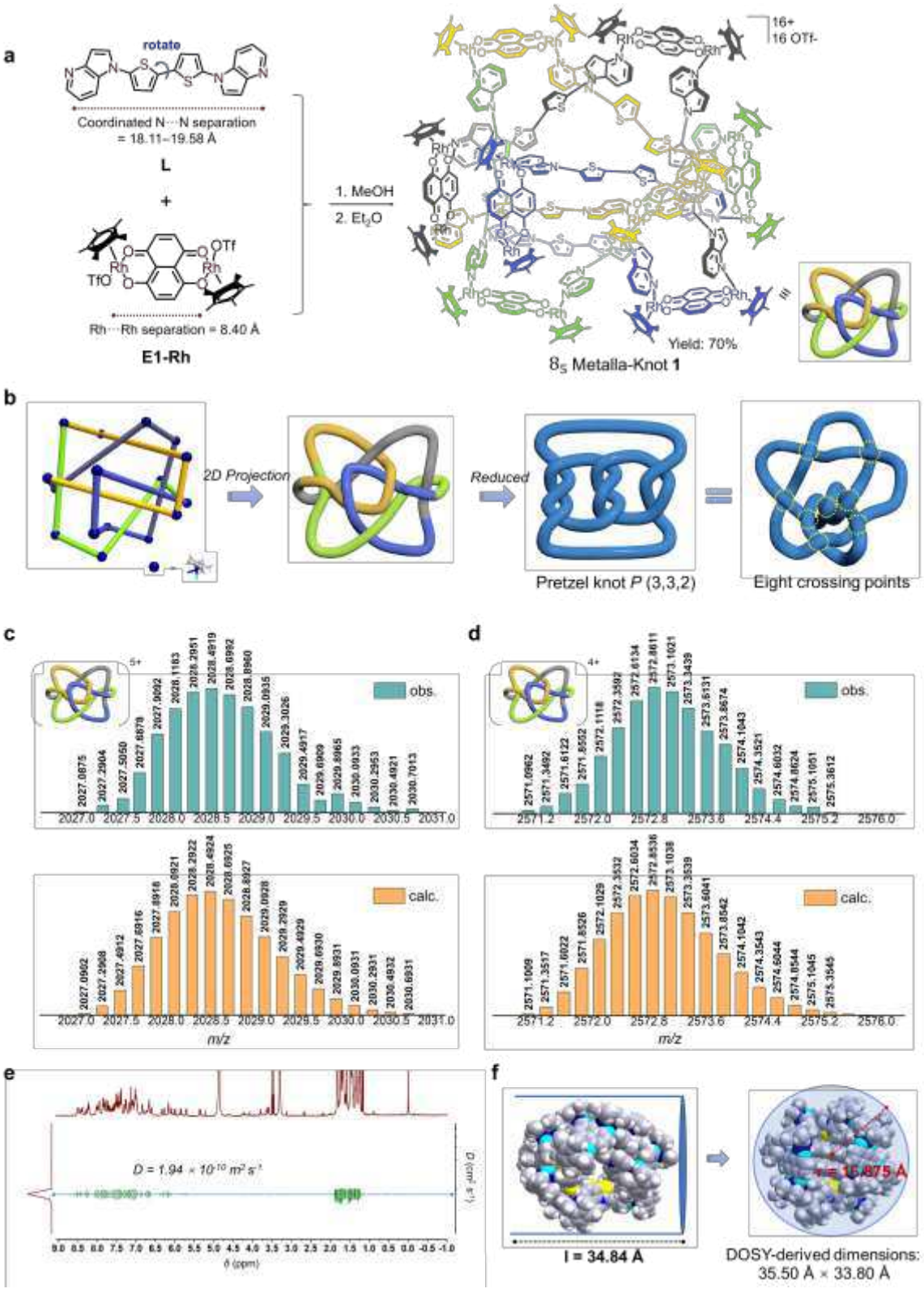


Fig. 3 | Design and synthesis of molecular 8_5 knot 1. a, Assembly of hexadecanuclear complex **1**. **b**, Reduced representation of 8_5 metalla-knot **1**. **c**, ESI-TOF/MS of **1** showing the observed distribution (top) and the calculated isotopic distribution (bottom) of [(**E1-Rh**)$_8$(**L**)$_8$](OTf$^-$)$_{11}$. **d**, ESI-TOF/MS of **1** showing the observed distribution (top) and the calculated isotopic distribution (bottom) of [(**E1-Rh**)$_8$(**L**)$_8$](OTf$^-$)$_{12}$. **e**, Partial ^{1}H DOSY NMR spectrum (400 MHz, 298.15K, c = 2.0 mM, $D = 1.94 \times 10^{-10}$ m^2 s^{-1}) of **1** in

methanol-d_4. **f**, DOSY-derived dimensions (height: l = 35.50 Å, diameter: d = 33.80 Å) fitted using diffusion constant $D = 1.94 \times 10^{-10}$ m^2 s^{-1} according to the cylinder model.

Within the ligand framework, face-to-face parallel stacking occurs between the electron-deficient 4-azaindolyl and the electron-rich bithiophene units within 3.51–3.84 Å, constituting an intramolecular donor–acceptor (D–A) charge-transfer π–π stacking interaction that provides key stabilization energy and helps to maintain the conformation of the 8_5 knot topology (Fig. 4g and Supplementary Fig. 40). Additionally, S···π and C–H···π interactions between bithiophene units of **L** and naphthyl of **E1-Rh** is also widely present in the skeleton (Fig. 4h). Two OTf^- anions reside within the central cavity of the assembly, stabilized by C–H···F and C–H···O interactions between the fluorine/oxygen atoms and the electron-poor aromatic C–H bonds (Supplementary Figs. 35 and 41). These non-covalent interactions are further corroborated by the independent gradient model (IGM) analysis based on the promolecular density[33-35](Fig. 4h).

To further elucidate the pronounced influence of the metal centre on the self-assembly outcome, we attempted to construct an analogous 8_5 knot architecture using the isoelectronic Cp*Ir^{III} fragment under otherwise identical conditions with ligand **L**. In stark contrast to the clean and selective formation of the Cp*Rh^{III}-containing 8_5 knot **1**, the corresponding Cp*Ir^{III}-mediated system yielded a complex mixture of species in solution. Despite extensive efforts to optimize the solvent composition, counteranions, concentration, and temperature, we could not isolate the target Cp*Ir^{III}-containing 8_5 knot and obtain diffraction-quality single crystals.

Size-directed topology assembly of 5_1 knot 2-M (M = Rh^{III}, Ir^{III})

The successful assembly of the unprecedented 8_5 knot from ligand **L** and the binuclear block **E1-Rh** relies on their exquisite size complementarity. This finely tuned, self-adaptive assembly process dictates the specific strand entanglement and the final topological outcome. We hypothesize that actively disrupting this size-matching equilibrium could compel the ligand to adopt a predominant conformation distinct from that observed in the 8_5 knot, thereby yielding alternative topological targets. To test this hypothesis, we employed the binuclear block **E2-M (M = Rh^{III}, Ir^{III})**, which features a longer M···M separation (8.75 Å) and an expanded conjugated π-surface. We aimed to perturb the original adaptive balance upon reaction with the same ligand **L**, thereby exploring the potential to access novel topological architectures.

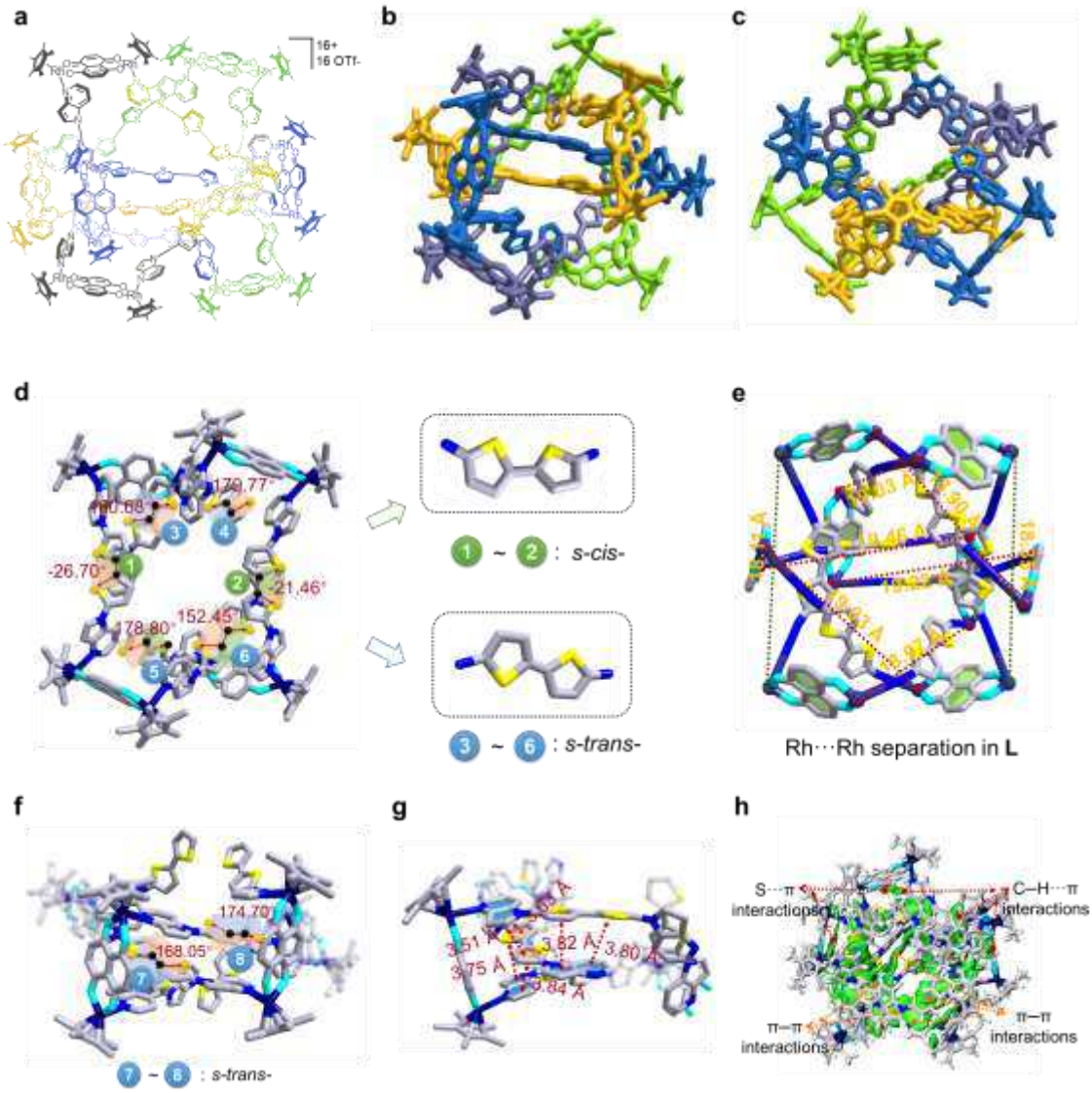


Fig. 4 | X-ray crystallographic analysis of 1. **a**, Chemical structure representation of molecular 8_5 knot, **1**. **b**, Structure of molecular 8_5 knot, **1** viewed along the *a* axis, and **c**, viewed along the *c* axis. **d**, Vertically aligned ligand strands of **1**. **e**, Rh···Rh separation in **L** of **1**. **f**, Horizontally aligned ligand strands of **1**. **g**, Partial structure highlighting inter-ring π–π stacking interactions in **1**. **h**, Intramolecular interaction visualizations of **1** by IGM analysis (isovalue = 0.003 a.u.). All triflate anions and solvent molecules were omitted for clarity. Color code: C, gray; N, navy blue; S, yellow; O, turquoise; H, white; Rh, blue.

First, the assembly of ligand **L** with an equimolar amount of **E2-Rh** at 24°C in methanol for 24h, followed by precipitation with diethyl ether, yielded a purple crystalline solid in a 75% yield (Fig. 5a). ESI-TOF/MS showed signal peaks at *m/z* 2202.4701 and 1614.6074, corresponding to the pentamer $[(\mathbf{E2\text{-}Rh})_5(\mathbf{L})_5](OTf^-)_n$ (n = 7, 6; Figs. 5c, 5d, and Supplementary Figs. 19–22) with the sequential loss of OTf^- counterions. The ^{1}H NMR spectrum of the product (methanol-d_4, 298.15K) exhibits sharp, highly symmetric resonances, with all five ligand strands in identical chemical

environments, consistent with a topology for **2-Rh** possessing five-fold symmetry (Supplementary Figs. 15–18). The precise topology and symmetry of **2-Rh**, determined by SCXRD, is that of a pentafoil knot (5_1) —also known as a cinquefoil knot or Solomon's seal knot with five crossing points. Conceptually, this 5_1 knot topology can be viewed as a deformation of the 8_5 knot topology with three crossing removed (Fig. 6a). Structurally, the five ligand strands intertwine in an alternating cross manner and are terminally capped via coordination to the binuclear block **E2-Rh**, furnishing a pentagram-like topological framework (Fig. 6b). In three-dimensional space, it features a well-defined central cavity with an inner radius of roughly 5.30 Å (Fig. 6b), alongside an outer peripheral thickness of approximately 21.67 Å. The results are consistent with the hydrodynamic size simulated from the diffusion coefficient $D = 2.25 \times 10^{-10}$ m^2 s^{-1} according to the cylinder model, confirming that the 5_1 knot maintains a compact, barrel-like geometry in both the solid and solution states (Figs. 6c and 6d).

The crystal structure of **2-Rh** reveals that all bithiophene moieties within the ligand strands exclusively adopt the *s-trans* conformation, in stark contrast to the conformational differentiation observed in **1** (Fig. 6e and Supplementary Fig. 36). This pronounced conformational homogenization provides direct evidence that the altered geometric parameters of the binuclear block from **E1-Rh** to **E2-Rh**, for example, the elongated Rh···Rh separation and the expanded conjugated π-surface, actively drive ligand **L** to adopt a fundamentally different dominant conformation during assembly, thereby redirects the self-assembly pathway away from the 8_5 knot and ultimately yielding the stable 5_1 knot as the thermodynamic product.

The stability of the 5_1 knot is predominantly driven by the π–π stacking interactions between the internal ligand strands and the anthracenyl planes of the binuclear block **E2-Rh**, alongside the C–H···π interactions among the ligand strands (Figs. 6f and 6g). Subsequently, the behaviour of **2-Rh** in solution was evaluated via variable-concentration ^{1}H NMR spectroscopy in methanol-d_4 ($0.05 - 2.0$ mM). The resulting spectra confirm the robust stability of the 5_1 knot topology in solution, showing no evidence of dissociation or structural rearrangement (Fig. 5b and Supplementary Fig. 31).

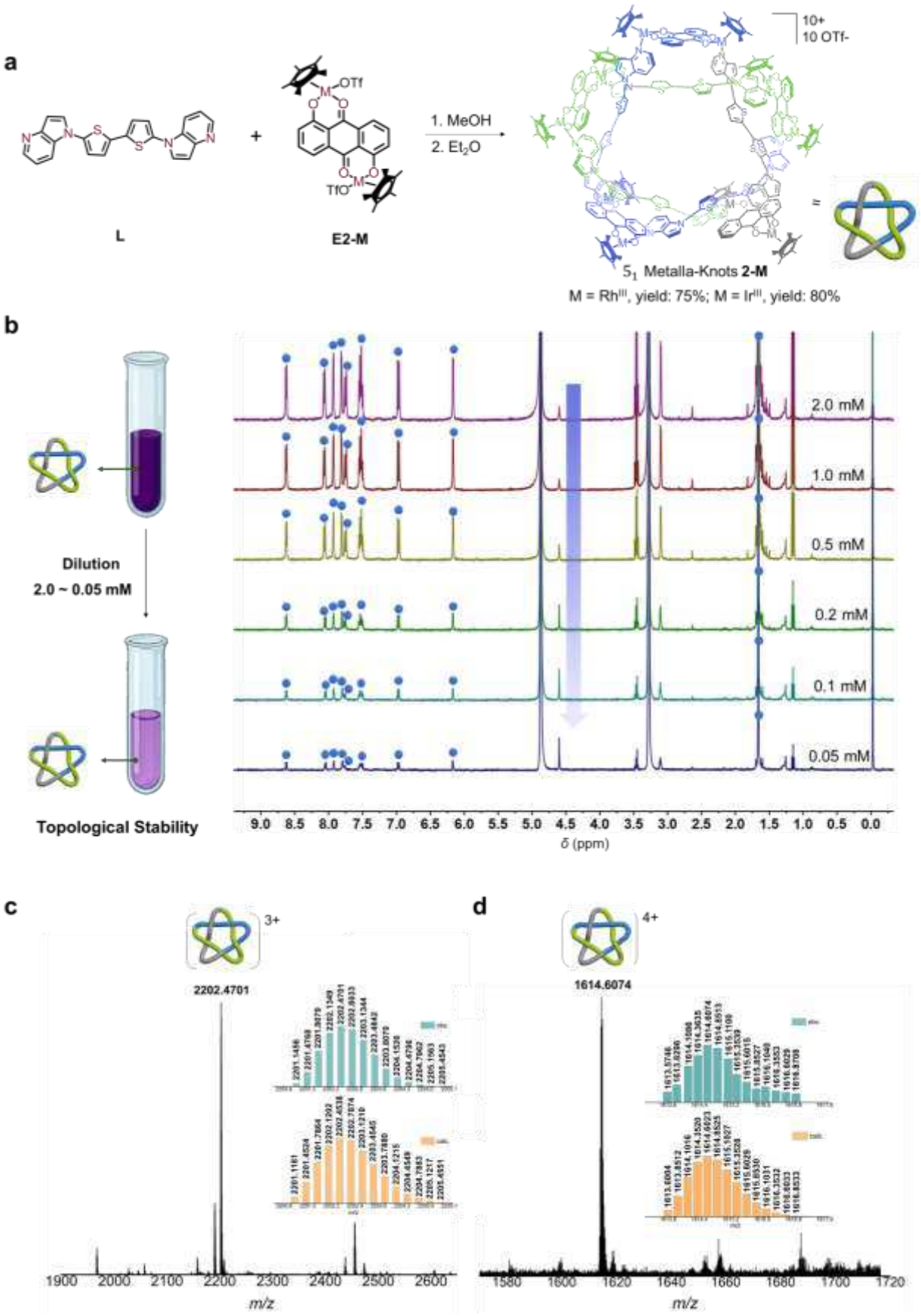


Fig. 5 | Formation of five-crossing molecular 5_1 knot 2-M. a, Synthesis of 5_1 metalla-knot **2-M**. **b**, variable-concentration ^{1}H NMR experiments (400 MHz, methanol-d_4, ppm, 298.15K) of **2-Rh**. **c**, and **d**,

ESI-TOF/MS of **2-Rh** with signals that correspond to the loss of various numbers of OTf^- anions. Calculated peaks (*m/z*): 2202.4701 [**2-Rh** – $3OTf^-$]$^{3+}$ and 1614.6074 [**2-Rh** – $4OTf^-$]$^{4+}$.

To further explore the effect of the metal centre on the topological stability of the 5_1 knot, we replaced Rh^{III} with Ir^{III}. Subjecting the binuclear block **E2-Ir** and ligand **L** to identical self-assembly conditions afforded an analogous Cp*Ir^{III}-containing 5_1 knot (**2-Ir**), and its precise topological structure was confirmed by SCXRD (Supplementary Figs. 37 and 38). X-ray diffraction analysis revealed that the topological framework of the 5_1 knot is primarily stabilized by a diverse array of intramolecular non-covalent interactions, including π–π stacking, C–H···π interactions, and S···π contacts (Supplementary Fig. 39). In addition, the overall assembly is further reinforced by complementary hydrogen-bonding interactions involving external OTf^- counteranions. IGM analysis corroborates the presence and significance of these weak non-covalent forces, providing clear theoretical support for the stabilization of this intricate molecular topology (Supplementary Figs. 43 and 44). The solution-state behavior and structural identity of **2-Ir** are unambiguously supported by one- and two-dimensional NMR spectroscopy alongside ESI-TOF/MS analysis (Supplementary Figs. 23–29).

Conclusion

In summary, we achieved the first chemical synthesis of the eight-crossing 8_5 knot **1**, filling a critical void in the landscape of complex molecular topologies. This elusive, entangled architecture was readily accessed via the rational design of a novel 4-azaindolyl-based ligand strand **L**, followed by coordination-driven self-assembly with the binuclear block **E1-Rh**. This 4-azaindolyl ligand possesses unique electronic and steric properties that decisively reroute self-assembly pathways away from conventional symmetric products towards challenging, low-symmetry targets. To demonstrate the broad applicability of the ligand platform, we systematically modulated the size of the building block **E** to selectively construct two novel 5_1 knots (**2-M**, where **M** = Rh^{III}, Ir^{III}). All three knots were unambiguously confirmed by X-ray crystallography, NMR spectroscopy, and ESI-TOF/MS. Overall, this work not only realizes the synthesis of the previously elusive 8_5 molecular knot but also demonstrates how subtle structural variations in assembly components can be harnessed to achieve tunable topological diversity.

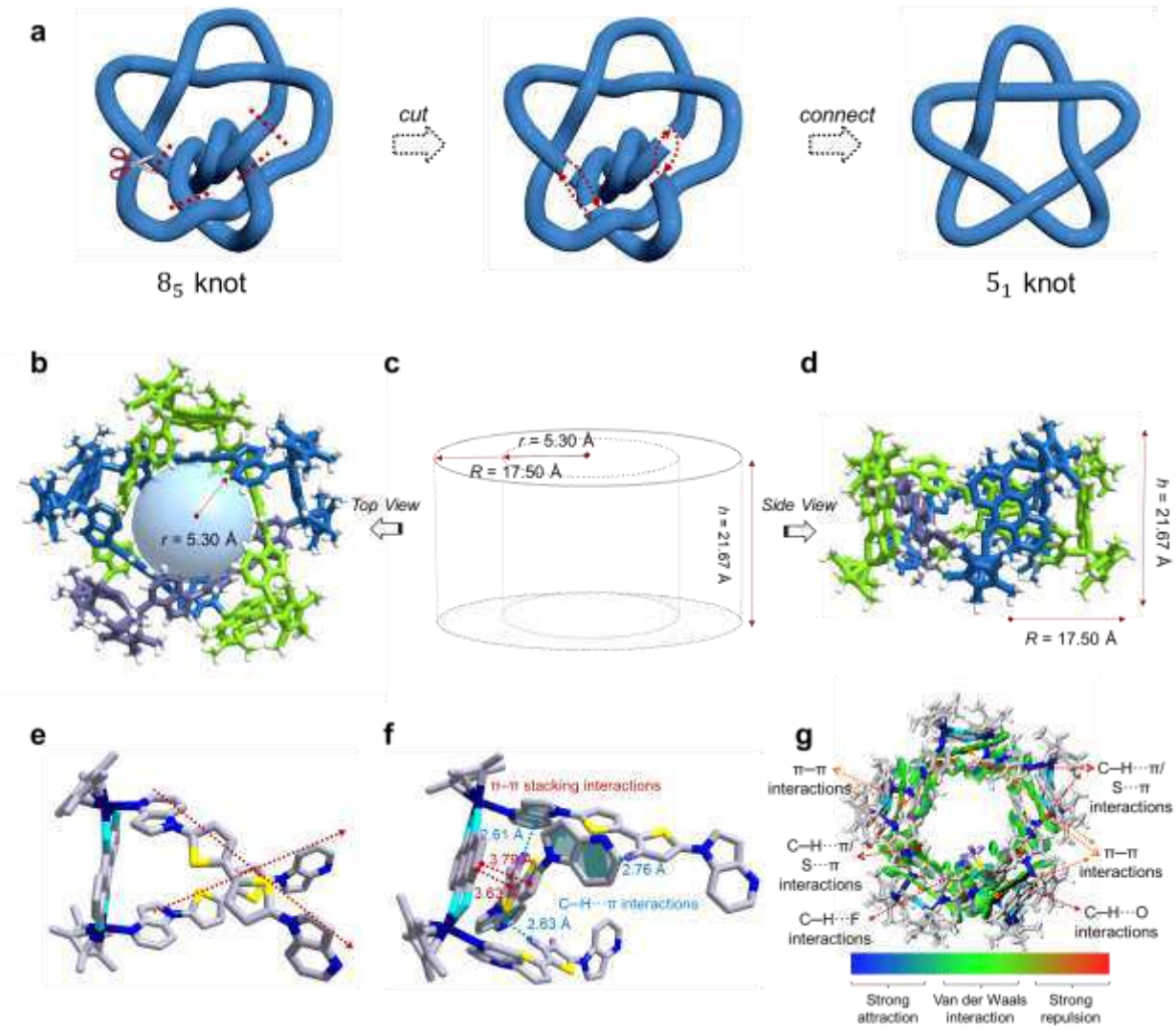


Fig. 6 | Topological analysis of molecular 5_1 knot. a, Comparison diagram of simplified topology and crossing points between 8_5 knot and 5_1 knot. **b**, Top view of **2-Rh**. **c**, Simulation diagram of the structure of **2-Rh**. **d**, Side view of **2-Rh**. **e**, The staggered pattern of ligand **L** in **2-Rh**. **f**, Partial non-covalent interactions in the structure of **2-Rh**. **g**, Intramolecular interaction visualizations of **2-Rh** by IGM analysis (isovalue = 0.003 a.u.). All triflate anions and solvent molecules were omitted for clarity. Color code: C, gray; N, navy blue; S, yellow; O, turquoise; H, white; Rh, blue.

Method

Synthesis: Ligand **L** was prepared through the Ullmann coupling reaction, and its synthetic protocols and characterization data are summarized in the Supporting Information. The 8_5 molecular knot **1** and two isostructural 5_1 knots (**2-Rh** and **2-Ir**) were separately assembled from ligand **L** in combination with the binuclear blocks **E1-Rh**, **E2-Rh,** and **E2-Ir**. Detailed synthetic procedures and systematic characterization of these topological architectures are also provided in the Supporting Information.

Computational details: Independent gradient model (IGM) analysis of promolecular density was performed for **1**, **2-Rh**, and **2-Ir**. The calculation model was established by extracting a molecule from the crystal structures. The cubic files (.cub) for IGM analysis[34,35] were generated by the wavefunction software Multiwfn 3.8[33], and the IGM inter-surfaces were visualized and analysed using the Visual Molecular Dynamics program (VMD 1.93)[36].

Data availability

Crystallographic data for the structures reported in this Article have been deposited at the Cambridge Crystallographic Data Centre, under deposition numbers CCDC 2545359 (**1**), 2545360 (**2-Rh**), and 2545489 (**2-Ir**). Copies of the data can be obtained free of charge via https://www.ccdc.cam.ac.uk/mystructures/. Other data that support the findings of this study are available in the Supplementary Information.

References

1. Forgan, R. S., Sauvage, J.-P. & Stoddart, J. F. Chemical topology: complex molecular knots, links, and entanglements. *Chem. Rev.* **111**, 5434–5464 (2011).
2. Ashbridge, Z., Fielden, S. D. P., Leigh, D. A., Pirvu, L., Schaufelberger, F. & Liang, Z. Knotting matters: orderly molecular entanglements. *Chem. Soc. Rev.* **51**, 7779–7809 (2022).
3. Stoddart, J. F. Dawning of the Age of Molecular Nanotopology. *Nano Lett.* **20**, 5597–5600 (2020).
4. Schlick, T. & Olson, W. K. Trefoil knotting revealed by molecular dynamics simulations of supercoiled DNA. *Science* **257**, 1110–1115 (1992).
5. Katsonis, N., Lancia, F., Leigh, D. A., Pirvu, L., Ryabchun, A. & Schaufelberger, F. Knotting a molecular strand can invert macroscopic effects of chirality. *Nat. Chem*. **12**, 939–944 (2020).
6. Tamura, Y., Takezawa, H. & Fujita, M. A Double-Walled Knotted Cage for Guest-Adaptive Molecular Recognition. *J. Am. Chem. Soc.* **142**, 5504–5508 (2020).
7. Rizzuto, F. & Nitschke, J. Stereochemical plasticity modulates cooperative binding in a CoII12L6 cuboctahedron. *Nat. Chem.* **9**, 903–908 (2017).
8. Gil-Ramírez, G., Hoekman, S., Kitching, M. O., Leigh, D. A., Vitorica-Yrezabal, I. J. & Zhang, G. Tying a molecular overhand knot of single handedness and asymmetric catalysis with the corresponding pseudo-D3-symmetric trefoil knot. *J. Am. Chem. Soc.* **138**, 13159–13162 (2016).
9. Yang, X., Chen, X., Yang, W. & Pommier, Y. Structural insights into human topoisomerase 3β DNA and RNA catalysis and nucleic acid gate dynamics. *Nat. Commun*. **16**, 834 (2025).
10. Alexander, J. W. & Briggs, G. B. On types of knotted curves. *Ann. Math.* **28**, 562–586 (1926).
11. Dietrich-Buchecker, C. O. & Sauvage, J.-P. A Synthetic Molecular Trefoil Knot. *Angew. Chem., Int. Ed. Engl.*, **28**, 189–192 (1989).
12. Gao, W.-X., Feng, H.-J., Guo, B.-B., Lu, Y. & Jin, G.-X. Coordination-Directed Construction of Molecular Links. *Chem. Rev.* **13**, 6288–6325 (2020).

13. Segawa, Y., Kuwayama, M., Hijikata, Y., Fushimi, M., Nishihara, T., Pirillo, J., Shirasaki, J., Kubota, N. & Itami, K. Topological molecular nanocarbons: all-benzene catenane and trefoil knot. *Science* **365**, 272–276 (2019).
14. Cui, Z. & Jin, G.-X. Construction of a molecular prime link by interlocking two trefoil knots. *Nat. Synth*. **1**, 635–640 (2022).
15. Li, Z., Zhang, J., Li, G. & Puddephatt, R. J. Self-assembly of the smallest and tightest molecular trefoil knot. *Nat. Commun*. **15**, 154 (2024).
16. Lu, Y., Li, Z.-J., Li, Y., An, L., Yang, S.-P. & Hahn, F. E. Observation of Near-Infrared Photothermal and Photoacoustic Effects in a Metallosupramolecular Trefoil Knot. *Angew. Chem. Int. Ed*. **64**, e202518415 (2025).
17. Ponnuswamy, N., Cougnon, F. B. L., Pantos, G. D. & Sanders, J. K. M. Homochiral and meso Figure Eight Knots and a Solomon Link. *J. Am. Chem. Soc.* **136**, 8243–8251 (2014).
18. Dang, L.-L., Sun, Z.-B., Shan, W.-L., Lin, Y.-J., Li, Z.-H. & Jin, G.-X. Coordination-Driven Self-Assembly of a Molecular Figure-Eight Knot and Other Topologically Complex Architectures. *Nat. Commun.* **10***,* 2057 (2019).
19. Ayme, J.-F., Beves, J. E., Leigh, D. A., McBurney, R. T., Rissanen, K. & Schultz, D. A synthetic molecular pentafoil knot. *Nat. Chem*. **4,** 15–20 (2012).
20. Inomata, Y., Sawada, T. & Fujita, M. Metal-Peptide Torus Knots from Flexible Short Peptides. *Chem* **6**, 294–303 (2020).
21. Danon, J. J., Krüger, A., Leigh, D. A., Lemonnier, J.-F., Stephens, A. J., Vitorica-Yrezabal, I. J. & Woltering, S. L. Braiding a molecular knot with eight crossings. *Science* **355**, 159–162 (2017).
22. Zhang, H.-N., Lin, Y.-J. & Jin, G.-X. Selective Construction of Very Large Stacking-Interaction-Induced Molecular 818 Metalla-knots and Borromean Ring Using Curved Dipyridyl Ligands. *J. Am. Chem. Soc.* **143**, 1119–1125 (2021).
23. Adams, C. C. The Knot Book: An Elementary Introduction to the Mathematical Theory of Knots, W. H. Freeman, New York, 1994.
24. Ghosh, K., Hu, J., White, H. S. & Stang, P. J. Construction of Multifunctional Cuboctahedra via Coordination-Driven Self-Assembly. *J. Am. Chem. Soc*. **131**, 6695–6697 (2009).
25. Xu, L., Wang, Y.-X., Chen, L.-J. & Yang, H.-B. Construction of multiferrocenyl metallacycles and metallacages via coordination-driven self-assembly: from structure to functions. *Chem. Soc. Rev*. **44**, 2148–2167 (2015).
26. Zhang, Y.-W., Zhang, H.-N., Wang, M.-X., Li, X. & Han, Y.-F. Sequence-encoded layered heteroleptic metalla-[2]catenanes for programmable supramolecular function. *Nat. Commun* **17***,* 1632 (2026).
27. Cui, Z., Hao, L.-Y., Yuan, Y.-F., Xuan, X.-P. & Jin, G.-X. Stereoselective Self-Assembly of a Topologically Chiral [6]Catenane with 18 Crossings. *Angew. Chem. Int. Ed.* e202515400 (2025).
28. Zhang, H.-N. & Jin, G.-X. Synthesis of molecular Borromean links featuring trimeric metallocages. *Nat. Synth*. **4**, 488–496 (2025).
29. Rong, Z., Chen, Z., Luong, F., Chheda, S., Luong, H. T. N., Zheng, Z., Greco, K., Alghamdi, A. A., Bui, K. H., Inizan, T. J., Nguyen-Dang, T., Pham, H. H., Le, D. D., Sauer, J., Phung, V. T., Chayes, J. T.,

Borgs, C., Boley, M., Ghaoui, L. E. & Yaghi, O. M. Algorithmic iterative reticular synthesis of zeolitic imidazolate framework crystals. *Nat. Synth* **5***,* 409–419 (2026).

30. Lee, Y., Nam, Y. S., Kim, S. Y., Ki, J. E. & Lee, H. G. Mechanistic duality of indolyl 1,3-heteroatom transposition. *Chem. Sci*. **14**, 7688–7698 (2023).
31. Tang, X., Zhang, W., Jiang, D.-X., Chen, Z., Shen, L., Tian, Y., Chen, J., Wang, Z. & Zeng, Y.-F. Access to Divergent Indolyl Pyrrolones via [3+2] Annulation of Indolyl Hydroxamates with Phosphonium Ylides. *Org. Lett.* **27**, 12137–12141 (2025).
32. Sarkar, N., Parkin, S. & Huckaba, A. J. Structural Study of Hydrogen-Bond Driven Cocrystallization of Pyridyl-Bithiophene Based Compounds. *Crystal Growth & Design* **21**, 4337–4345 (2021)
33. Lu, T. & Chen, F. Multiwfn: a multifunctional wavefunction analyzer. *J. Comput. Chem* **33**, 580–592 (2012).
34. Lefebvre, C., Rubez, G., Khartabil, H., Boisson, J.-C., Contreras-García, J. & Hénon, E. Accurately extracting the signature of intermolecular interactions present in the NCI plot of the reduced density gradient versus electron density. *Phys. Chem. Chem. Phys*. **19**, 17928–17936 (2017).
35. Lu, T. & Chen, Q. Independent gradient model based on Hirshfeld partition: a new method for visual study of interactions in chemical systems. *J. Comput. Chem.* **43**, 539–555 (2022).
36. Humphrey, W., Dalke, A. & Schulten, K. VMD: visual molecular dynamics. *J. Mol. Graphics* **14**, 33–38 (1996).

Acknowledgements

This work was supported by the National Science Foundation of China (21720102004, 224B2104, 22031003) and the Shanghai Science Technology Committee (Grant No. 2024ZDSYS02). G.-X. J. thanks the Alexander von Humboldt Foundation for a Humboldt Research Award.

Author contributions

Y. Z., H. T., and G.-X. J. designed the experimental protocol. Y. Z. and H. T. completed the synthesis and characterization studies, calculations, solved the crystal structure, and wrote the manuscript. G.-X. J. directed the research. Y. Z., H. T., and G.-X. J revised the manuscript.

Competing interests

Authors declare that they have no competing interests.

Supplementary Files

This is a list of supplementary files associated with this preprint. Click to download.

- 1.cif
- 2Ir.cif
- 2Rh.cif
- Supportinginformation.docx